Journal of Tropical Resources and Sustainable Science
Website : http://journal.umk.edu.my/index.php/jtrss/
eISSN : 2462-2389
Vol: SI Issue 1, 2025, 162-173
DOI: https://doi.org/10.47253/jtrss.v13i3.2013

RESEARCH ARTICLE

Assessing landslide susceptibility in Bukit Kwong dam, Kelantan, Malaysia using geospatial techniques and frequency ratio model

Nasuha Ishak[1*], Wani Sofia Udin[1,2], Esra'a Fawaz Alaeed[3] and Shadi Hanandeh[3]

[1]Faculty of Earth Science, Universiti Malaysia Kelantan, Jeli Campus, 17600 Jeli, Kelantan, Malaysia
[2]Tropical GeoResource & Hazards Research Group, Faculty of Earth Science, Universiti Malaysia Kelantan, Jeli Campus, 17600 Jeli, Kelantan, Malaysia
[3]Department of Civil Engineering, Al-Balqa Applied University, As-Salt 191117, Jordan

ARTICLE HISTORY
Received: 22 July 2025
Accepted: 30 October 22025
Online: 31 December 2025

KEYWORDS
Landslide susceptibility,
Unmanned Aerial Vehicles,
Frequency ratio model,
Area under curve,
Malaysia

☒ * **CORRESPONDING AUTHOR**
Sr. Gs. Nasuha binti Ishak
Faculty of Earth Science,
Universiti Malaysia Kelantan (Jeli Campus), 17600 Jeli, Kelantan, Malaysia.
Email: nasuhaishak21@gmail.com

ABSTRACT

Landslides occurring at or near dam structures are among the predominant forms of geological hazards responsible for significant loss of life, property damage, and environmental degradation worldwide. To understand the risk, this study evaluates the landslide susceptibility in the nearly ageing Bukit Kwong Dam where ageing denotes to time-related deterioration occurring fifty years of operation using an integrated approach of Unmanned Aerial Vehicles (UAV), Geographic Information System (GIS) and frequency ratio model selected due to its simplicity and ability to provide numerical measure of the relative importance in the landslide occurrence. The proposed methodology involves the preparation of a landslide inventory, generation of multiple thematic maps representing factors influencing slope instability, including aspect, slope, plan curvature, profile curvature, elevation, land use, distance from river, Normalized Difference Vegetation Index (NDVI), rainfall, and distance from road. These thematic layers were subsequently integrated within a GIS environment using the frequency ratio technique to produce a Landslide Susceptibility Map (LSM). The LSM delineated five susceptibility classes, ranging from very low (48%), low (34%), moderate (12%), high (5%), and very high (1%). According to their high frequency values, slope, land use, plan and profile curvatures, and distance from river were identified as the most influential predisposing factors contributing to landslide occurrence. The performance and accuracy were evaluated using Area Under Curve (AUC), yielding a score of 0.85. The outcomes provide useful baseline information to identify landslide-prone areas for dam safety evaluations and slope management strategies in the region.

1. INTRODUCTION

Globally, numerous dam failures have been reported, both during the construction phase (Celik and Gul, 2021) and operation (Shrestha and Kawasaki, 2020). Most dams are located within rugged mountainous and gorge regions characterized by complex geological settings, highly variable material composition, and steeply inclined bank slopes. The steep and unstable slopes in such regions often trigger landslide-induced surges, which can subsequently cause dam overtopping (Dong et al., 2021). Additionally, the slow evolution of landslides in the dam area can be triggered by excessive rainfall or nearby deforestation and cause debris flows (Chang et al., 2022; Fan et al., 2020; Yang et al., 2022; Zheng et al., 2021; Zhong et al., 2021; Zhu et al., 2020).

However, the study of potential landslides within the dam area in Malaysia is quite unusual and has not received the necessary attention. It is a concern given that the average age of dams in Malaysia has exceeded 40 years, and are mostly made of earthfill or rockfill materials, which is also known as embankment dams (MyDAMS, 2017). The embankment dams are structures composed of natural materials such as soil, clay, and rockfill which are less cohesive and weaker than concrete (Wieland, 2023). These materials are more susceptible to internal erosion, saturation, and shear failure on slopes (Fan et al., 2021). Rapid deposition of these materials caused by landslides can potentially block rivers, resulting in flooding and posing a significant danger (Zhong et al., 2021). Over time, material deterioration, environmental factors, and operational stress can affect its performance and stability (Fan et al., 2021; Wieland, 2023). A dam is considered ageing after approximately fifty years of operation, although large dams in harsh environments may experience ageing effects earlier (Wieland, 2023). The vulnerability of ageing dams requires careful monitoring. Comprehending the dynamic behavior and forecasting potential of the hazard chains resulting from

landslide failure is important for improving risk reduction and emergency preparedness.

Susceptibility mapping is the key component of landslide prediction and risk assessment by defining the potential for landslide occurrence with the correlation of landslide inventory comprising data on historical landslide occurrences as well as causative factors (Moragues et al., 2024). In general, the causative factors can be further categorized into 2 groups: (1) triggering parameters (due to environmental factors and human engineering activities) and conditioning parameters (due to topographic factors and geological factors) (Mersha and Meten, 2020). These factors can be obtained from secondary data sources; however, it is essential to ensure the acquired data are up to date and at the highest possible spatial resolution to enhance the reliability of the analysis. In this sense, Unmanned Aerial Vehicles (UAV) offer the capability to capture detailed surface information in centimeter level spatial resolution, which can be processed to derive key inputs such as slope, aspect, land cover, and significantly aid in the accuracy of the landslide susceptibility map (LSM) (Tempa et al., 2021).)

LSM can be derived using statistical methods, including the frequency ratio model (FRM) (Yuvaraj and Dolui, 2021; Moragues et al., 2024; Babitha et al., 2022; Das and Lepcha, 2019). This method is widely adopted for calculating factor weights in Geographic Information System (GIS) based analyses due to simpler implementation and less bias compared to qualitative methods such as weightage based on expert opinion (Asmare, 2023; Thiery et al., 2020). Additionally, the influence of each causative factor can be determined based on the calculated frequency ratio (FR) values associated with each factor class. Model comparison for accuracy assessment indicated that LSM using the FRM has proven dependable and consistently outperforms other models (Das and Lepcha, 2019; Babitha et al., 2022).

This study primarily aims to develop a landslide susceptibility map for Bukit Kwong Dam, Kelantan, Malaysia, and to enhance the accuracy by utilizing mainly UAV-derived products as the main source of input data for causative factors. Detection of regions at risk of landslides within the dam allows a better understanding of the actual ground conditions and the essential preventive actions to be taken.

2. MATERIALS AND METHODS

2.1. Study area

The Bukit Kwong Dam, located southwest of Rantau Panjang in the Pasir Mas district of Kelantan, serves as the study area (Figure 1). Commissioned in 1979, it is a nearly ageing embankment dam constructed using earth fill and rip-rap materials. The dam comprises three principal structures, including a gated semi-circular service spillway, main dam body, and irrigation intake system. It has a total storage capacity of 14.3 million cubic meters and a catchment area covering approximately 11 square meters. In accordance with International Commission on Large Dams (ICOLD) classification standards, Bukit Kwong Dam is categorized as a high hazard potential structure.

The topography is moderately dissected hilly with vegetated valleys and steep, linear ridges adjacent to the reservoir embankment. The region is underlain by riverine alluvial soils that are vulnerable to slope failure due to their loose texture and low compaction. Furthermore, the precipitation is significantly influenced by the northeast monsoon that typically brings heavy and prolonged rainfall during the period of November and March. The intense precipitation in the region has strong potential to initiate landslides, consistent with observations at Batu Arang dam during the 1981 incident (MyDAMS, 2017).

The study area has experienced localized instability, with minor soil slip reported on the downstream slope in 2019. Seepage has also been observed occasionally, with occurrences being more prominent during the rainy season. The elevated seepage discharge can cause pressure on the slopes, leading to changes in instability and potential landslides. In addition, illegal deforestation was reported in the surrounding hilly areas, which may alter surface runoff and reduce slope reinforcement provided by vegetation. Collectively, these hazard factors heighten the risk of landslides, thereby threatening dam safety and the integrity of the reservoir.

2.2 Landslide inventory map

The map of landslide inventory shows past landslides in the area that may contain information such as locations, depth of the landslide, volume of the landslide, blocking river, and landslide damage (Yuvaraj and Dolui, 2021). This information is vital to investigate the mechanism of landslide failure by assessing the spatial pattern of landslide occurrences and relevant conditioning factors (Dhungana et al., 2023). In this study, the identification of landslide locations relied on the site inspection report provided by the Department of Irrigation and Drainage (DID), Malaysia, in the period of 2018 to 2024, as well as field observations. The landslides were identified in 48 locations (Figure 1), primarily characterized by structural cracking as well as soil and rock flow movements that occurred after intense rainfall. The locations were split into 70% training data to generate LSM and 30% testing data for validation through random selection using GIS ArcGIS Pro software. The allocation of the training dataset and test dataset was selected based on the majority covered by literatures (Khanna et al., 2021; Dhungana et al., 2023; Zhao and Chen, 2019).

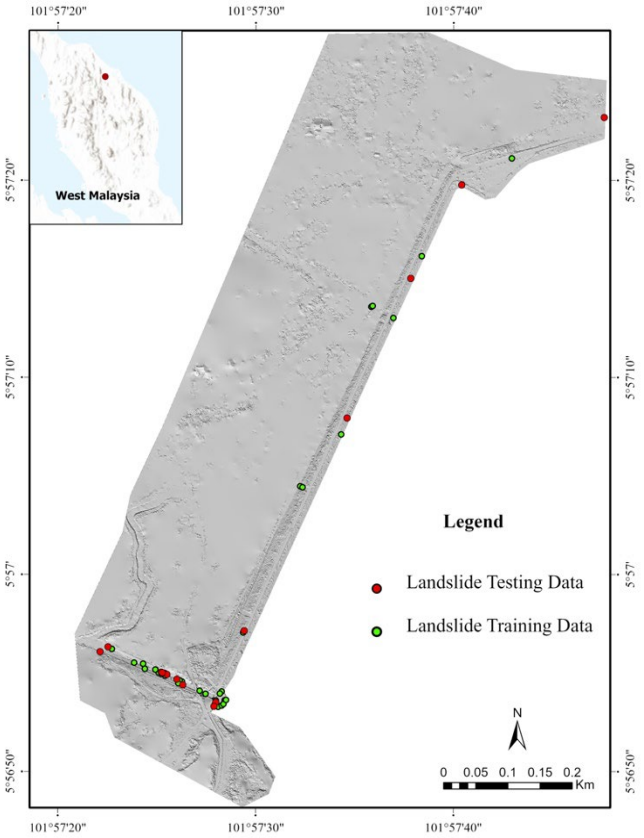

Figure 1: Shaded relief of the Bukit Kwong dam in Malaysia showing 48 landslide locations randomly divided into testing and training data. Note: Shaded relief was generated using UAV imagery.

2.3 Landslide causative factors

The selection of causative factors was guided by reviewing studies with similar general characteristics of the study area (e.g. dam site area) (Zhao et al., 2024; Feng et al., 2025), tropical country (Sholichin et al., 2024), as well as per landslide studies in Malaysia (Abubakar et al., 2025; Yusof et al., 2024; Selamat et al., 2022). Furthermore, the selection was also guided by the accessibility of data for this study area. Ten parameters were selected and categorized into three main aspects, such as topography factors, environmental factors, and human activities factors. The preliminary results from a previous study by Ishak and Udin (2024), based on UAV-derived Digital Elevation Model (DEM) and orthomosaic, at resolution of 9.34 centimeter and 2.34 centimeter, respectively served as the primary input for extracting the parameters listed in Table 1. Geological factors such as soil type and lithology were not considered in the analysis, as these characteristics are relatively uniform across the study area and therefore do not significantly influence the spatial variations in landslide susceptibility (Kincey et al., 2024). The Bukit Kwong Dam foundation is primarily composed of highly permeable riverine alluvial soils. The underlying lithology is predominantly of schist and gneiss of Permian age and consists mainly of weak fine-grained rocks such as phyllite, slate, and shale. The subordinate lithologies include sandstone, schist, limestone, and volcanic rocks from rhyolitic to andesitic composition.

Aspect is an essential topographical factor that characterizes the orientation of the slope and determines the received degree of solar radiation, which modifies the rock and soil moisture, thereby indirectly affecting the slope stability (Panchal and Shrivastava, 2022). In this study, aspects were classified into 10 classes and resampled using the nearest neighbour. Another crucial topographic factor is slope. It can be directly associated with landslides, which can cause a slope failure (Panchal and Shrivastava, 2022). The slope with a higher angle is typically more vulnerable to collapse, which is strongly associated with landsliding processes (Dhungana et al., 2023). Slope was divided into 6 classes based on natural break classification. While the standard classification scheme established by the Department of Mineral and Geoscience Malaysia for hill land remains useful for standard design comparability, the natural break classification helps to preserve natural thresholds in heavily skewed topographic data and better reflect the local frequency distribution of the study area and thereby enhancing the interpretability of model outputs (Zhao et al., 2021; Xiao et al., 2025). As topographical metrics, plan and profile curvature describe the geomorphic structures of the terrain and slope, influencing landslide occurrence primarily through their control on erosion and surface runoff processes (Tyagi et al., 2022). The plan curvature controlled the direction of landslide movement, which controls the degree of convergence or divergence of landslide materials along the slope (Panchal and Shrivastava, 2022). Meanwhile, the profile curvature dynamically affected the forces acting within a landslide along the slope direction (Panchal and Shrivastava, 2022). In the case of both curvatures, the classification was made for negative values indicating concave surfaces, zero values denote flat areas, and positive values correspond to convex surfaces. Lastly, elevation was included because in high relief terrain, factors like vegetation coverage, rainfall, and human activities are highly correlated with elevation, which exposed to the risk of landslide occurrence (Asmare, 2023). This factor was derived from the DEM and reclassified into 4 classes using bilinear interpolation.

Land use is one of the environmental factors used to understand better specific land uses in different regions, whether commercial built area, natural forest, vegetation area, residential or plantation area (Shirzadi et al., 2019). The land use of the area can subsequently change over time due to significant implications for ecosystems, climate change, global biogeochemical cycles, and human vulnerability. This study extracted the land use from the orthomosaic by UAV using a supervised maximum likelihood classifier into 6 classes.

Rainfall is the most triggering environmental parameter for landslide occurrence globally, as it changes with geographical variations and climatic conditions that affect the frequency and intensity of precipitation in the region (Panchal and Shrivastava, 2022). Intense rainfall events elevate pore water pressure and affect the soil moisture, thereby reducing slope stability, which results in landslides (Asmare, 2023). This study used a cubic interpolation between the Bukit Kwong rainfall station and the nearest rainfall station from 2017 to 2024. The rainfall map was classified into 5 classes. Another environmental factor is the distance to river as it affects the soil moisture accumulated at the lower portions of the slopes, leading to saturation and a consequent reduction in slope stability (Loche et al., 2022). The Normalized Difference Vegetation Index (NDVI) parameter is used to represent the growth state and coverage of vegetation, which provides a huge influence on the weathering of slope, runoff, and the seepage (Tempa et al., 2021). Both the distance to river and the NDVI parameters were obtained from the produced orthomosaic derived by the UAV. The value of NDVI ranges from -1 to +1 and can be figured using Equation 1:

$$NDVI = (NIR - R)/(NIR + R) \quad (1)$$

where, R means red band in a UAV aerial image and NIR means a band near infrared.

Lastly, the distance from the road suggests human activity that altered the natural topography terrain and induced the slope instability, such as road clear-cutting and construction activities (Asmare, 2023). This study used orthomosaic as a reference to digitize the road shapefiles and used the Euclidean Distance spatial analysis tool in ArcGIS Pro to develop the map.

The thematic maps were rasterized at a 10 centimeters resolution to correspond with the spatial resolution of the UAV products. The horizontal spatial reference was set to Geocentric Datum of Malaysia (GDM2000) Kelantan Grid (EPSG3385), and heights were derived based on the MyGeoid vertical datum. GIS ArcGIS software was used for spatial management and data analysis.

2.4 General methodology

This study constructed the methodology in four main steps: (1) development of landslide inventory, (2) preparation of thematic maps, (3) generation of landslide susceptibility map, and (4) validation assessment, as shown in Figure 2. The data was mainly derived from the UAV and other sources to obtain necessary information, including causative factors and inventory (Table 1).

Table 1: Summary of the data and their sources

Factors	Triggering/conditioning parameters	Source
Landslide inventory		Field observation, Department of Irrigation and Drainage (DID), Malaysia
Topography	Aspect	UAV-derived DEM
	Slope	UAV-derived DEM
	Plan curvature,	UAV-derived DEM
	Profile curvature,	UAV-derived DEM
	Elevation	UAV-derived DEM
Environmental	Land use,	UAV-derived Orthomosaic
	Distance to river,	UAV-derived Orthomosaic
	NDVI,	UAV-derived Orthomosaic
	Rainfall	Department of Irrigation and Drainage (DID), Malaysia
Human activity	Distance to road	UAV-derived Orthomosaic

GIS tools were used to classify factor categories and quantify their statistical correlation with the spatial distribution of historical landslides. The ratio between pixels associated with causative factors and pixels corresponding to landslide occurrence was obtained using Equation (2) (Sonker and Tripathi, 2022).

$$\text{Frequency ratio (FR)} = \frac{p/q}{r/s} \quad (2)$$

where,

p = number of landslide occurrences within each class of a factor

q = total number of landslide occurrences within the study area

r = number of pixels in a given factor class where landslides have occurred

s = total number of pixels representing the entire study area

After that, the obtained FR values are normalized using the following Equation (3) (Sonker and Tripathi, 2022). For each factor, the Prediction Rate (PR) was subsequently calculated as per Equation (4) (Moragues et al., 2024).

$$FR_n = \frac{FR}{\Sigma \text{Class FR}} \quad (3)$$

$$PR = (FR_{n\ max} - FR_{n\ min})/ (FR_{n\ max} - FR_{n\ min}) \text{ Min} \quad (4)$$

where, FR_n represents the spatial association coefficient (relative frequency) between each factor and landslide occurrences, and PR denotes the prediction rate.

Finally, the Landslide susceptibility map (LSM) was generated by combining the classes of ten factors with their relative frequency ratio values. The weighted sum of these ten parameters was integrated using the proposed algorithm, and the computation was performed as described in Equation 5 (Moragues et al., 2024)

$$LSM = \Sigma\ (WC * PR) \quad (5)$$

where, WC represents the Weighting Coefficients of the ten parameters, and PR refers to the prediction rate, while LSM denotes the Landslide Susceptibility Map.

Validation of the generated susceptibility map was carried out using the Area under the ROC curve (AUC) based on the testing dataset. Equation 6 was used to compute the ROC curve (Moragues et al., 2024):

$$\text{ROC} = \frac{\Sigma \text{TP} + \Sigma TN}{P+N} \quad (6)$$

where, true positive (TP) are defined as correctly classified landslide pixels, true negative (TN) are defined as correctly classified non-landslide pixels, and P and N are defined as the number of landslide and non-landslide, respectively.

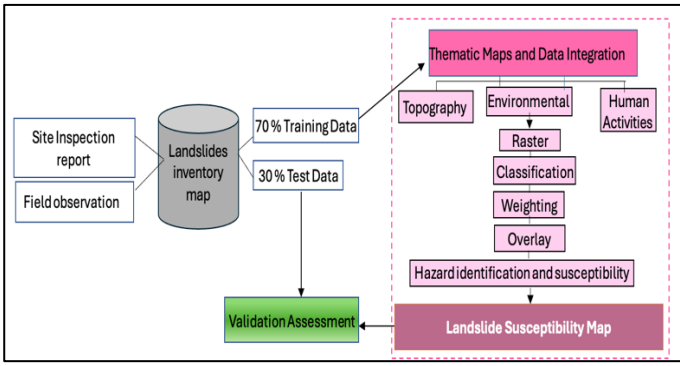

Figure 2: The workflow of methodology used in this study consisted of four main steps: 1) preparation of landslide inventory, 2) development of thematic map, 3) generation of landslide susceptibility map, and 4) validation assessment.

3. RESULT AND DISCUSSION

3.1. Frequency ratio model analysis

In this study, ten different thematic maps were created, such as slope, aspect, plan and profile curvature, elevation, land use, distance to river, NDVI, distance to road, and rainfall map, as presented in Figure 3. The relationship between a landslide causative factor and landslide occurrence can be characterized using FRM. The FR values for each class of all thematic maps were calculated and disclosed in Table 2. An FR value exceeding 1 generally signifies a positive association between the respective class and the occurrences of landslide (Tempa et al., 2021). Based on the obtained FR values (Table 2), each parameter is discussed below.

(a) **Slope**. The 48-87° slope class recorded the highest FR value (32.29), higher among all classes across the evaluated parameters. This indicates that this class has the strongest correlation with landslide occurrence in the study area. Other classes, such as 12- 21°, 22-32° and 33-47° have FR values of 3.11, 2.03, and 2.43 respectively. The lowest correlation is 0-4° with 0.26 FR value, followed by 5-11° with 0.91.

(b) **Aspect**. The most landslide points are in the north, followed by the west direction. Meanwhile, in the southeast direction, no landslide point is observed. The flat (FR = 1.47), east (FR = 0.44), west (FR = 0.86), south (FR = 1.11), and northwest (FR = 0.97) have low to moderate correlation to landslide occurrence. The northeast shows the best correlation among all with 1.95 FR value.

(c) **Profile curvature**. The study area consisted mostly of flat surfaces, with 94.15 % of class pixels. The concave surface dominantly influenced the landslide occurrence of the parameter with 13.19 FR value.

(d) **Plan curvature**. Similarly, the flat terrain occupied the horizontal curvature, with 96.94%. A high correlation is observed for the concave slope with 13.72 FR value and 6.15 FR value for the convex slope.

(e) **Elevation**. The lowest correlation is found in high relief terrain with 27 - 32 meter class. In the classes of 23 - 24 meter and 25 - 26 meter, the FR value is 0.88 and 1.07 respectively. Meanwhile, the highest correlation is < 22 class (FR value = 1.91). This shows that landslide occurrence decreases with an increase in elevation in the study area.

(f) **Rainfall**. All classes in the rainfall parameters are not significantly varied and are below 2.0 FR value. The highest FR value (1.86) is seen in the 3500 – 3699 millimeter/year (mm/yr) class, while the lowest (0.38) is in the 3900 – 3999 mm/yr class.

(g) **NDVI**. The class of 0.26 – 0.38 has the highest correlation (FR value = 3.42) between landslide occurrence and total area. In second place is -0.03 – 0.10 class with 1.67 FR value. Zero correlation is found in the 0.50 – 0.60 class, which has the highest class pixels (46.88%). The 0.11 – 0.25 class and 0.39 – 0.49 class have the average FR values of 0.84 and 0.98, respectively.

(h) **Land use**. Agriculture has the highest class pixels (42.18%) in the study area, but has a low correlation to landslide occurrence (FR = 0.07). The built-up area scored the highest FR value with 10.35, a huge gap with other classes. Forest area showed no association with landslide occurrence, while shrubland exhibited only a weak correlation (FR value = 0.18). Water class is usually river and reservoir in the study area, has quite a high correlation with landslide occurrence, with 3.02 FR value.

(i) **Distance to river**. This parameter exhibited the highest FR value (6.14) in the < 5 meter class and significantly decreased with an increase in distance to river. Beyond 25 meters, no substantial landslide occurrence was observed.

(j) **Distance to road**. All classes show medium to low correlation to landslide occurrence, with the highest 20 meter class (FR value = 3.23), followed by < 5 meter (FR value = 3.13), 15 meter (FR value = 2.51), 10 meter (FR value = 1.26), 25 meter (FR value = 0.70), and lastly <250 meter (FR value + 0.48).

Table 2: Frequency ratio values of ten landslide causative factors.

Parameters	Classes	Pixels	Pixels (%) [a]	Landslide points	Landslide points (%) [b]	Frequency ratio [b/a]
Slope (°)	0-4	23802498	68.69	6.00	18.18	0.26
	5-11	5749158	16.59	5.00	15.15	0.91
	12-21	2360157	6.81	7.00	21.21	3.11
	22-32	1552761	4.48	3.00	9.09	2.03
	33-47	864482	2.49	2.00	6.06	2.43
	48-87	325176	0.94	10.00	30.30	32.29
Aspect	Flat	2147419	6.20	3.00	9.09	1.47
	North	6139100	17.72	10.00	30.30	1.71
	Northeast	2154942	6.22	4.00	12.12	1.95
	East	2395023	6.91	1.00	3.03	0.44
	Southeast	2226905	6.43	0.00	0.00	0.00
	South	2828544	8.16	3.00	9.09	1.11
	Southwest	4031161	11.63	1.00	3.03	0.26
	West	7326388	21.14	6.00	18.18	0.86
	Northwest	5404750	15.60	5.00	15.15	0.97
Profile Curvature	Concave	318671	0.92	4.00	12.12	13.19
	Flat	32655022	94.15	19.00	57.58	0.61
	Convex	1709557	4.93	10.00	30.30	6.15
Plan Curvature	Concave	382985	1.10	5.00	15.15	13.72
	Flat	33623425	96.94	23.00	69.70	0.72
	Convex	676840	1.95	5.00	15.15	7.76
Elevation (m)	< 22	6602683	19.04	12.00	36.36	1.91
	23-24	11957820	34.48	10.00	30.30	0.88
	25-26	8881189	25.61	9.00	27.27	1.07
	27-32	7241558	20.88	2.00	6.06	0.29
Rainfall (mm/yr)	3500-3699	6230212	17.96	11.00	33.33	1.86
	3700-3799	10931024	31.52	10.00	30.30	0.96
	3800-3899	8302691	23.94	8.00	24.24	1.01
	3900-3999	5490819	15.83	2.00	6.06	0.38
	4000-4400	3728504	10.75	2.00	6.06	0.56
NDVI	-0.03-0.10	3185131	9.09	5.00	15.15	1.67
	0.11-0.25	3803424	10.85	3.00	9.09	0.84
	0.26-0.38	6207439	17.72	20.00	60.61	3.42
	0.39-0.49	5416990	15.46	5.00	15.15	0.98
	0.50-0.6	16427016	46.88	0.00	0.00	0.00
Land use	Water	1043788	3.01	3.00	9.09	3.02
	Built-up area	2233168	6.44	22.00	66.67	10.35
	Barren land	4912811	14.16	6.00	18.18	1.28
	Forest	6066902	17.49	0.00	0.00	0.00
	Scrubland	5798379	16.72	1.00	3.03	0.18
	Agriculture	14628028	42.18	1.00	3.03	0.07
Distance to river (m)	< 5	2053148	5.92	12.00	36.36	6.14
	10	2023903	5.84	3.00	9.09	1.56
	15	1993321	5.75	2.00	6.06	1.05
	20	1929325	5.56	0.00	0.00	0.00
	25	1874821	5.41	2.00	6.06	1.12
	< 250	24808726	71.53	14.00	42.42	0.59
Distance to road (m)	< 5	2697373	7.75	8.00	24.24	3.13
	10	2513975	7.22	3.00	9.09	1.26
	15	2103836	6.04	5.00	15.15	2.51
	20	1631991	4.69	5.00	15.15	3.23
	25	1513212	4.35	1.00	3.03	0.70
	> 250	24344541	69.95	11.00	33.33	0.48

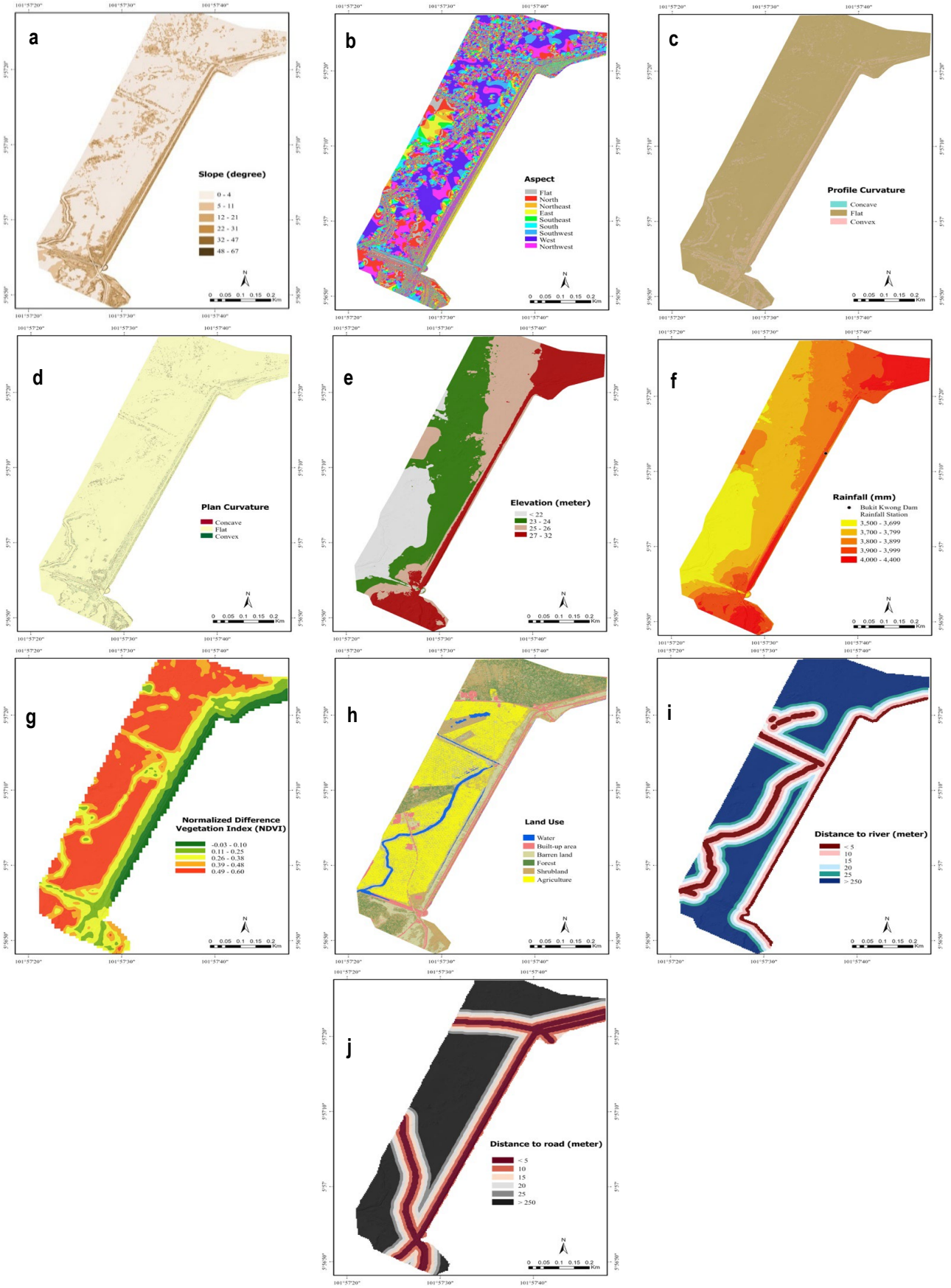

Figure 3: Thematic maps for landslide causative factors implicated in the study area. (a) Slope (°) showing steep gradients concentrated along the dam flanks and rivers, (b) Aspect showing distinct in slope orientation, (c) Profile curvature predominantly in flat surface, (d) Plan curvature also reflecting mostly flat, (e) Elevation (meter) with higher altitude located in the southern and corner area, (f) Rainfall (millimeter/year) decreasing gradually away from the dam, (g) NDVI indicating dense vegetation across much of the area, (h) Land use dominated by agricultural land, (i) Distance to river (meter) concentrated near the center of study area and (j) Distance to road (meter) showing roads primarily located near the dam.

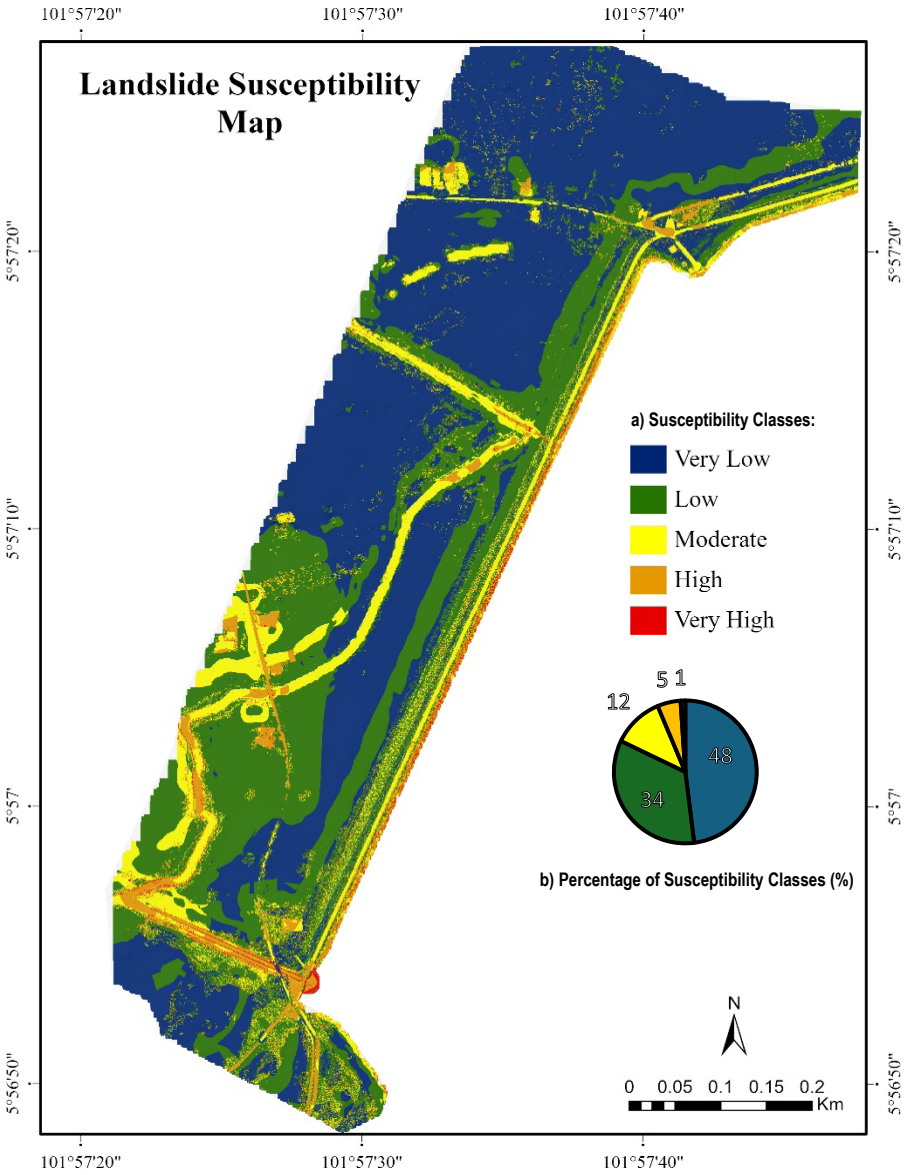

Figure 4: (a) Landslide susceptibility map using FRM in Bukit Kwong Dam. The areas of very low, low, and moderate zones across most of the study area. The landslide prone areas are concentrated near hydraulic structures, water bodies, and nearby infrastructures. (b) Percentage distribution of susceptibility in each class, with nearly three-quarters of the study area falls within the very low to moderate susceptibility categories, while high and very high zones occupied comparatively limited area.

3.2. Landslide susceptibility map and validation

The study classified the generated LSM into five classes, such as very low, low, moderate, high, and very high using natural breaks as illustrated in Figure 4 (a). Nearly 48% of the study area was identified as belonging to the very low landslide susceptibility (Figure 4b), predominantly covering regions characterized by forest and agricultural land use. This is further supported by the 0.50-0.60 NDVI class, which represents dense vegetation, where no correlation with landslide occurrence was identified, indicating the stabilizing effect of well-vegetated areas. Dense vegetation can serve as a natural buffer, reducing the direct impact of rainfall on slopes and thereby mitigating the potential for landslide initiation (Huangfu et al., 2024). Areas of low (34%) and moderate susceptibility (12%) are found mostly in the upper part of the study area, where the elevation is usually low, from 22 to 26 meters, and lower slope angles (below 21°). The land use for these areas is shrubland, water, and some built-up areas such as roads. The high (5%) and very high (1%) susceptibility are located near the spillway, reservoir bank, river, main canal, embankment dam, as well as in proximity to buildings, bridges, and roads. A similar pattern has been observed at the Karun-3 Dam, where elevated susceptibility occurs along the riverbanks, lakeshores, dam structures, and adjacent road networks (Zandi and Far, 2025).

In this study, the highest susceptibility (high and very high) occurs between 48° to 87° slope angles, built-up land use, concave profile and plan curvature area, proximity to the river (< 5 meters), and to a lesser extent, areas located within 20 meters of a road. Oliveira et al. (2024) reported that slopes

exceeding 45° in hilly terrain are highly susceptible to landslide initiation, particularly combined with weak or weathered lithologies. In Peninsular Malaysia, 27% of 37 documented landslide cases were triggered in sedimentary rock formations such as limestone and shale (Maturidi et al., 2021). Steep gradients in the present study could exert greater force on unconsolidated alluvial underlain by weathered schist and limestone that promote downslope transport of loose materials, resulting in the accumulation of mixed rock and soil deposits. This explains the frequent occurrences of such deposits near the sump area. Furthermore, the influence of concave curvature may also facilitate additional material accumulation. Slope stability is critically influenced by curvature, as the accumulation of water and loose materials is promoted by concave structures, increasing pressure of pore water and reducing shear strength, thereby making slopes more susceptible to failure (Moragues et al., 2024). Similarly, in other studies, very highly susceptible zones are commonly associated with slopes exceeding 30° (Moragues et al., 2024; Ngo et al., 2021; Hakim et al., 2022; Asmare, 2023; Sonker and Tripathi, 2022), urban areas where land disturbance is pronounced (Thein et al., 2023; Ngo et al., 2021), concave curvatures (Selamat et al., 2022; Dam et al., 2022), as well as distance within 300 meter of road and river (Sonker and Tripathi, 2022; Asmare, 2023).

The PR value was calculated to describe the relative weight or influence of each causative factor on the landslide occurrence based on FR values (Moragues et al., 2024). Analysis of the PR values for each weighted factor demonstrates that slope (4.017), land use (3.572), profile curvature (3.246), distance to river (3.021), and plan curvature (3.014) have the highest weight as shown in Figure 5. These findings imply that topographic form and environmental factors exert stronger spatial control on slope instability and have dominantly shaped the LSM model, as evidenced by their cumulative FR values in the study. Notably, slope consistently ranks as the most significant factor in LSM (Shano et al., 2021; Moragues et al., 2024; Boukhres et al., 2023). Land use also plays a critical role in slope stabilization through the reinforcing effects of root systems (Ngo et al., 2021). Surface cover and vegetation density are determined by the type of land use, which in turn modifies surface hydrology and soil properties, thereby affecting the likelihood of landslides (Xiao et al., 2025). Slopes that remain unaffected by landslides are primarily at higher elevations (above 25 meters) within the northeast and southwest oriented valley corners, where dense forest cover dominates. The presence of a dense vegetation canopy serves as natural protective barrier from the direct impact of rainfall on the surface of the soil. This relationship is evident by moderate PR values of 2.550 for NDVI and 2.012 for elevation, which suggest that vegetation cover and elevation provide stabilizing effects against landslide occurrence in the study area. In addition, profile and plan curvatures also influence slope response to instability. Concave profile curvatures enhance water concentration along the slope, while concave plan curvature facilitates sediment accumulation with deposits commonly observed along the valley bottoms where landslides frequently initiate (Lin et al., 2021; Selamat et al., 2022; Moragues et al., 2024).

In other high-altitude studies, such as Choke Mountain (Asmare, 2023), Sikkim Himalaya (Sonker and Tripathi, 2022), Three Gorges Reservoir (Zhou et al., 2025), and Karaj Dam (Asadi Nalivan et al., 2024), the main landslide predisposing factors are distance to rivers, distance to road, and slope. Here, the river occupies the central valley bottom, where high and very high susceptibility zones are concentrated. Occasional seepage along the riverbanks near the downstream area may have increased soil saturation levels due to elevated moisture content. Fluctuation of water levels and increased flow velocities, especially during intense rainfall, may reduce shear strength in soils, promoting slope failure. In Malaysia, rainfall was often identified as the most triggering factor, such as in Langat River Basin (Selamat et al., 2022), Muda River Basin (Abubakar et al., 2025), and Penang Island (Yusof et al., 2024), as well as in a similar tropical climate, such as Konto Watershed, Indonesia (Sholichin et al., 2024). Interestingly, rainfall (PR value = 1.587) does not appear to play a major role in triggering landslides in this context, possibly due to nearly uniform precipitation distribution in the study area. Moreover, in detailed or small-scale susceptibility studies (e.g. map scale finer than 1:500), the variation of rainfall thresholds is often minimal, reducing the relative influence compared to geomorphological and geological factors (Maturidi et al., 2021). Meanwhile, the lowest PR weights were observed for distance to road and aspect with 1.256 and 1.00, respectively, indicating minor significance on the number of landslides occurrences. This may be attributed to the absence of active constructions nearby that could alter natural geology, drainage patterns, or impose additional loads affecting soil stability (Moragues et al., 2024). Moreover, the roads in the study area are generally service roads, small and located at a considerable distance from the slopes. Aspect exhibited a low influence, likely because the slope orientations in this study do not significantly vary in solar radiation, moisture retention, and vegetation density that could affect the instability of the slope (Saranaathan et al., 2021).

The accuracy of the LSM model was assessed using the AUC derived from the ROC curve. The curve measures the capability of the model to accurately distinguish between true positives and negatives cases within the testing dataset. The predictive performance of the model is reflected by the AUC value, which ranges from 0 to 1, with higher accuracy indicated by values closer to 1. Specifically, an AUC of 1.0 represents a perfect model, 0.90-0.99 denotes excellent performance, 0.8-0.89 indicates good model, 7-0.79 suggests fair performance, 0.51-0.69 implies poor performance, while values of 0.5 or below indicates no predictive ability (Boukhres et al., 2023; Das and Lepcha, 2019; Shano et al., 2021; Moragues et al., 2024).

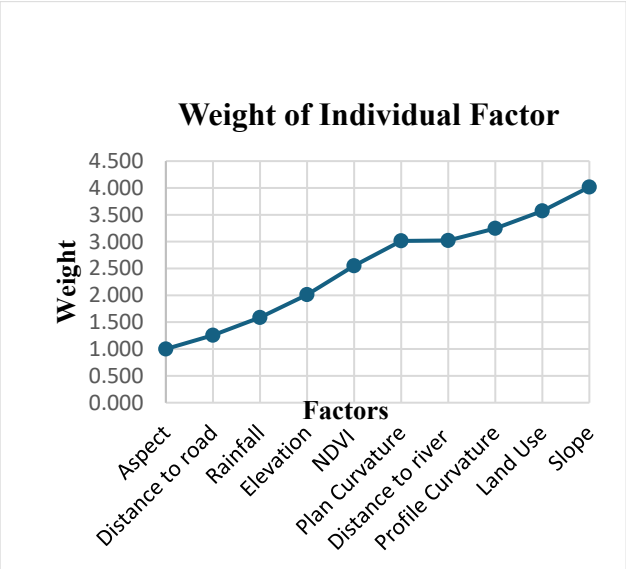

Figure 5: The PR value indicating the weight of the individual factor in the LSM model, showing the slope as the dominant predictor, with land use, profile curvature, distance to river, and plan curvature also contributing notably.

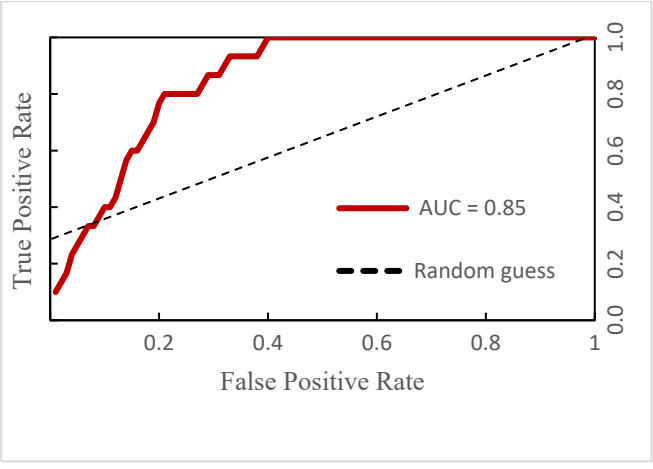

Figure 6: FRM model evaluation performance from the ROC curve showing an estimated model accuracy of about 85%.

The successive rate of FRM in this study was 0.85 (Figure 6), which is considered a good test and shows a high predictive landslide occurrence as reported by Mallick et al. (2021). Other landslide susceptibility studies (Ngo et al., 2020; Sonker and Tripathi, 2022; Asmare, 2023) reported comparable results, whereas slightly lower performance was reported by Moragues et al. (2024) and Hakim et al. (2021).

4. CONCLUSION

The susceptibility map in this study is the result of a combination relationship between ten selected causative factors: aspect, slope, elevation, profile, and plan curvature, rainfall, NDVI, land use, distance to river and road using the frequency ratio model. The UAV based data acquisition contributed significantly to the successful extraction of parameters for the landslide susceptibility map. The study shows that landslide susceptibility is dominated by very low to moderate landslide susceptibility. Only approximately 6% of the area was identified as part of high to very high susceptibility categories, indicating limited zones with significant landslide risk. These susceptible areas are primarily situated in built-up areas, on steeper slopes (48 – 87°), concave profile and plan curvature, and a distance less than 5 meters to the river. The strongest predictors in the study area, according to the predictive values are slope, land use, profile and plan curvatures, and distance to river. The performance of the landslide susceptibility map is considered a good test with an accuracy of 0.85. The derived results of this study may serve as an important reference for local authorities in decision making process and for researchers interested in identifying influential factors in similar study areas within Malaysia.

ACKNOWLEDGEMENT

The authors gratefully acknowledge Ms. Habibahatikah binti Abdullah and Mohammad bin Ab Rahman from the Department of Irrigation and Drainage (DID), Pasir Mas District, for their support and helpful guidance during the site visit throughout the study.

REFERENCES

Abubakar, S., Abir, I. A., Rahman, R. A., & Muztaza, N. M. (2025). Landslide susceptibility analysis of the Kampung Iboi, Muda River Basin, Kedah, Malaysia using remote sensing, 2d-resistivity and GIS. *Advances in Space Research*.

Asadi Nalivan, O., Rahmani, M., Vakili Tajareh, F., & Bayat, A. (2024). Prioritization of factors and zoning susceptibility of landslide in Karaj Dam Watershed. *Watershed Engineering and Management*, *16*(1), 1-15.

Asmare, D. (2023). Application and validation of AHP and FR methods for landslide susceptibility mapping around Choke Mountain, Northwestern Ethiopia. *Scientific African*, 19, e01470.

Babitha, B., Danumah, J. H., Pradeep, G., Costache, R., Patel, N., Prasad, M. K., Rajaneesh, A., Mammen, P. C., Ajin, R., & Kuriakose, S. L. (2022). A framework employing the AHP and FR methods to assess the landslide susceptibility of the Western Ghats region in Kollam district. *Safety in Extreme Environments*, 4(2), 171-191.

Bhagya, S. B., Sumi, A. S., Balaji, S., Danumah, J. H., Costache, R., Rajaneesh, A., & Abioui, M. (2023). Landslide susceptibility assessment of a part of the Western Ghats (India) employing the AHP and F-AHP models and comparison with existing susceptibility maps. *Land*, 12(2), 468.

Boukhres, N., Mastere, M., Thiery, Y., Maquaire, O., El Fellah, B., & Costa, S. (2023). A comparative modeling of landslides susceptibility at a meso-scale using frequency ratio and analytic hierarchy process models in geographic information system: the case of African Alpine Mountains (Rif, Morocco). *Modeling Earth Systems and Environment*, *9*(2), 1949-1975.

Celik, E., & Gul, M. (2021). Hazard identification, risk assessment and control for dam construction safety using an integrated BWM and MARCOS approach under interval type-2 fuzzy sets environment. *Automation in Construction*, 127, 103699.

Chang, M., Luo, C., Wu, B., & Xiang, L. (2022). Catastrophe process of outburst debris flow triggered by the landslide dam failure. *Journal of Hydrology*, 609, 127729

Dam, N. D., Amiri, M., Al-Ansari, N., Prakash, I., Le, H. V., Nguyen, H. B. T., & Pham, B. T. (2022). Evaluation of Shannon entropy and weights of evidence models in landslide susceptibility mapping for the Pithoragarh district of Uttarakhand state, India. *Advances in Civil Engineering*, *2022*(1), 6645007.

Das, G., & Lepcha, K. (2019). Application of logistic regression (LR) and frequency ratio (FR) models for landslide susceptibility mapping in Relli Khola river basin of Darjeeling Himalaya, India. *SN Applied Sciences*, 1, 1-22.

Dhungana, G., Ghimire, R., Poudel, R., & Kumal, S. (2023). Landslide susceptibility and risk analysis in Benighat Rural Municipality, Dhading, Nepal. *Natural Hazards Research.*

Dong, K., Li, Z., Lu, X., Chen, C., Sheng, J., Chen, J., & Wu, Z. (2021). Analysis of dam overtopping failure risks caused by landslide-induced surges considering spatial variability of material parameters [Original Research]. *Frontiers in Earth Science*, 9. https://doi.org/10.3389/feart.2021.675900

Fan, X., Dufresne, A., Whiteley, J., Yunus, A. P., Subramanian, S. S., Okeke, C. A. U., Pánek, T., Hermanns, R. L., Ming, P., Strom, A., Havenith, H.-B., Dunning, S., Wang, G., & Tacconi Stefanelli, C. (2021). Recent technological and methodological advances for the investigation of landslide dams. *Earth-Science Reviews*, 218, 103646. https://doi.org/https://doi.org/10.1016/j.earscirev.2021.103646

Fan, X., Yunus, A. P., Scaringi, G., Catani, F., Siva Subramanian, S., Xu, Q., & Huang, R. (2021). Rapidly evolving controls of landslides after a strong earthquake and implications for hazard assessments. *Geophysical Research Letters*, *48*(1), e2020GL090509.

Feng, Z. Y., Zhou, J. W., Yang, X. G., Tan, L. J., & Liao, H. M. (2025). Prediction of landslide dam stability and influencing factors analysis. *Engineering Geology*, 350, 108021.

Hakim, W. L., Rezaie, F., Nur, A. S., Panahi, M., Khosravi, K., Lee, C. W., & Lee, S. (2022). Convolutional neural network (CNN) with metaheuristic optimization algorithms for landslide susceptibility mapping in Icheon, South Korea. *Journal of environmental management*, *305*, 114367.

Huangfu, W., Qiu, H., Wu, W., Qin, Y., Zhou, X., Zhang, Y., & He, Y. (2024). Enhancing the performance of landslide susceptibility mapping with frequency ratio and gaussian mixture model. *Land,* 13(7), 1039

Ishak, N., & Udin, W. S. (2024). Mapping embankment dam geomorphology using unmanned aerial vehicles (UAVs): a case study of Bukit Kwong dam, Kelantan, Malaysia. BIO Web of Conferences (Vol. 131, p. 04007). *EDP Sciences.*

Kincey, M. E., Rosser, N. J., Swirad, Z. M., Robinson, T. R., Shrestha, R., Pujara, D. S., & Dunant, A. (2024). National-scale rainfall-triggered landslide susceptibility and exposure in Nepal. *Earth's Future*, *12*(2), e2023EF004102.

Khanna, K., Martha, T. R., Roy, P., & Kumar, K. V. (2021). Effect of time and space partitioning strategies of samples on regional landslide susceptibility modelling. *Landslides*, 18, 2281-2294.

Lee, S., & Pradhan, B. (2007). Landslide hazard mapping at Selangor, Malaysia using frequency ratio and logistic regression models. *Landslides*, *4*(1), 33-41.

Lin, Q., Lima, P., Steger, S., Glade, T., Jiang, T., Zhang, J., & Wang, Y. (2021). National-scale data-driven rainfall induced landslide susceptibility mapping for China by accounting for incomplete landslide data. *Geoscience Frontiers*, *12*(6), 101248.

Loche, M., Alvioli, M., Marchesini, I., Bakka, H., & Lombardo, L. (2022). Landslide susceptibility maps of Italy: Lesson learnt from dealing with multiple landslide types and the uneven spatial distribution of the national inventory. *Earth-Science Reviews*, 104125.

Malaysia Dam Safety Management Guidelines (MyDAMS) (2017)

Mallick, J., Alqadhi, S., Talukdar, S., AlSubih, M., Ahmed, M., Khan, R. A., & Abutayeh, S. M. (2021). Risk assessment of resources exposed to rainfall induced landslide with the development of GIS and RS based ensemble metaheuristic machine learning algorithms. *Sustainability,* 13(2), 457.

Maturidi, A. M. A. M., Kasim, N., Taib, K. A., Azahar, W. N. A. W., & Tajuddin, H. B. A. (2021). Empirically based rainfall threshold for landslides occurrence in Peninsular Malaysia. *KSCE Journal of Civil Engineering*, *25*(12), 4552-4566.

Moragues, S., Lenzano, M. G., Jeanneret, P., Gil, V., & Lannutti, E. (2024). Landslide susceptibility mapping in the Northern part of Los Glaciares National Park, Southern Patagonia, Argentina using remote sensing, GIS and frequency ratio model. *Quaternary Science Advances*, 13, 100146.

Mersha, T., & Meten, M. (2020). GIS-based landslide susceptibility mapping and assessment using bivariate statistical methods in Simada area, northwestern Ethiopia. *Geoenvironmental disasters*, 7(1), 1-22.

Ngo, P. T. T., Panahi, M., Khosravi, K., Ghorbanzadeh, O., Kariminejad, N., Cerda, A., & Lee, S. (2021). Evaluation of deep learning algorithms for national scale landslide susceptibility mapping of Iran. *Geoscience Frontiers*, *12*(2), 505-519.

Oh, H. J., & Pradhan, B. (2011). Application of a neuro-fuzzy model to landslide-susceptibility mapping for shallow landslides in a tropical hilly area. *Computers & geosciences*, 37(9), 1264-1276.

Oliveira, S. C., Zêzere, J. L., Garcia, R. A., Pereira, S., Vaz, T., & Melo, R. (2024). Landslide susceptibility assessment using different rainfall event-based landslide inventories: advantages and limitations. *Natural Hazards*, *120*(10), 9361-9399.

Panchal, S., & Shrivastava, A. K. (2022). Landslide hazard assessment using analytic hierarchy process (AHP): A case study of National Highway 5 in India. *Ain Shams Engineering Journal*, *13*(3), 101626.

Saranaathan, S. E., Mani, S., Ramesh, V., & Prasanna Venkatesh, S. (2021). Landslide susceptibility zonation mapping using bivariate statistical frequency ratio method and GIS: a case study in part of SH 37 Ghat Road, Nadugani, Panthalur Taluk, The Nilgiris. *Journal of the Indian Society of Remote Sensing*, *49*(2), 275-291.

Selamat, S. N., Majid, N. A., Taha, M. R., & Osman, A. (2022). Landslide susceptibility model using artificial neural network (ANN) approach in Langat river basin, Selangor, Malaysia. *Land*, *11*(6), 833.

Shano, L., Raghuvanshi, T. K., & Meten, M. (2021). Landslide susceptibility mapping using frequency ratio model: the case of Gamo highland, South Ethiopia. *Arabian Journal of Geosciences*, *14*(7), 623.

Shirzadi, A., Solaimani, K., Roshan, M. H., Kavian, A., Chapi, K., Shahabi, H., Keesstra, S., Ahmad, B. B., & Bui, D. T. (2019). Uncertainties of prediction accuracy in shallow landslide modeling: Sample size and raster resolution. *Catena*, *178*, 172-188.

Sholichin, M., Othman, F., Prayogo, T. B., & Rahardjo, S. S. P. (2024). Assessing Landslide susceptibility and formulating adaptation strategies in the Konto Watershed, East Java, Indonesia. *International Journal of Disaster Risk Reduction*, *113*, 104797.

Shrestha, B. B., & Kawasaki, A. (2020). Quantitative assessment of flood risk with evaluation of the effectiveness of dam operation for flood control: A case of the Bago River Basin of Myanmar. *International Journal of Disaster Risk Reduction*, 50, 101707.

Sonker, I., & Tripathi, J. N. (2022). Remote sensing and GIS-based landslide susceptibility mapping using frequency ratio method in Sikkim Himalaya. *Quaternary Science Advances*, *8*, 100067.

Tempa, K., Peljor, K., Wangdi, S., Ghalley, R., Jamtsho, K., Ghalley, S., & Pradhan, P. (2021). UAV technique to localize landslide susceptibility and mitigation proposal: a case of Rinchending Goenpa landslide in Bhutan. *Natural Hazards Research,* 1(4), 171-186.

Thein, K. S. M., Nagai, M., Nakamura, T., Phienwej, N., & Pal, I. (2023). Assessment of the Impacts of Urbanization on Landslide Susceptibility in Hakha City, a Mountainous Region of Western Myanmar. *Land*, *12*(5), 1036. https://doi.org/10.3390/land12051036

Thiery, Y., Terrier, M., Colas, B., Fressard, M., Maquaire, O., Grandjean, G., & Gourdier, S. (2020). Improvement of landslide hazard assessments for regulatory zoning in France: state–of–the-art perspectives and considerations. *International Journal of Disaster Risk Reduction*, 47, 101562.

Tyagi, A., Tiwari, R. K., & James, N. (2022). A review on spatial, temporal and magnitude prediction of landslide hazard. *Journal of Asian Earth Sciences: X*, *7*, 100099.

Wieland, M. (2023). Ageing and life-span of dams. In *Role of Dams and Reservoirs in a Successful Energy Transition* (pp. 989-995). CRC Press.

Xiao, T., Huang, W., Wang, L., Yang, B., Qin, Z., Liu, X., & Xiao, Y. (2025). Uncertainty-aware ensemble learning and dynamic threshold optimization for landslide susceptibility mapping. *Computers & Geosciences*, 106042.

Yang, Y., Chen, G., Meng, X., Bian, S., Chong, Y., Shi, W., Jiang, W., Jin, J., Li, C., & Mu, X. (2022). Analysis of the microseismicity characteristics in landslide dam failure flume tests: implications for early warning and dynamics inversion. *Landslides,* 19(4), 789-808.

Yuvaraj, R. M., & Dolui, B. (2021). Statistical and machine intelligence-based model for landslide susceptibility mapping of Nilgiri district in India. *Environmental Challenges*, 5, 100211.

Zandi, R., & Far, G. S. P. (2025). Evaluating the factors affecting landslides using machine learning algorithms (case study: the catchment area of Karun-3 Dam, Iran). *The Egyptian Journal of Remote Sensing and Space Sciences*, *28*(3), 512-522.

Zhou, C., Gan, L., Cao, Y., Wang, Y., Segoni, S., Shi, X. & Singh, R. P. (2025). Landslide susceptibility assessment of the Wanzhou district: Merging landslide susceptibility modelling (LSM) with InSAR-derived ground deformation map. *International Journal of Applied Earth Observation and Geoinformation*, *136*, 104365.

Zhao, F., Miao, F., Wu, Y., Ke, C., Gong, S., & Ding, Y. (2024). Refined landslide susceptibility mapping in township area using ensemble machine learning method under dataset replenishment strategy. *Gondwana Research*, 131, 20-37.

Zhao, X., & Chen, W. (2019). GIS-based evaluation of landslide susceptibility models using certainty factors and functional trees-based ensemble techniques. *Applied Sciences*, 10(1), 16.

Zhao, Z., Liu, Z. Y., & Xu, C. (2021). Slope unit-based landslide susceptibility mapping using certainty factor, support vector machine, random forest, CF-SVM and CF-RF models. *Frontiers in Earth science*, *9*, 589630.

Zheng, H., Shi, Z., Shen, D., Peng, M., Hanley, K. J., Ma, C., & Zhang, L. (2021). Recent advances in stability and failure mechanisms of landslide dams. *Frontiers in Earth Science*, 9, 659935.

Zhong, Q., Wang, L., Chen, S., Chen, Z., Shan, Y., Zhang, Q., Ren, Q., Mei, S., Jiang, J., & Hu, L. (2021). Breaches of embankment and landslide dams-State of the art review. *Earth-Science Reviews*, 216, 103597.

Zhu, X., Peng, J., Liu, B., Jiang, C., & Guo, J. (2020). Influence of textural properties on the failure mode and process of landslide dams. *Engineering Geology,* 271, 105613.

